

CLINICAL STUDY



Noninvasive grading of renal interstitial fibrosis and prediction of annual renal function loss in chronic kidney disease: the optimal solution of seven MR diffusion models

Guanjie Yuan^a, Zhouyan Liao^a, Ping Liang^a, Lingli Cai^a, Kailun Zhou^a, Ting Yin^b, Wei Chen^b, Omar Darwish^c, Chuou Xu^a, Min Han^d and Zhen Li^a

^aDepartment of Radiology, Tongji Hospital, Tongji Medical College, Huazhong University of Science and Technology, Wuhan, Hubei, China; ^bMR Research Collaboration Team, Siemens Healthineers Ltd., Shanghai, China; ^cMR Application Predevelopment, Siemens Healthcare, Erlangen, Germany; ^dDepartment of Nephrology, Tongji Hospital, Tongji Medical College, Huazhong University of Science and Technology, Wuhan, Hubei, China

ABSTRACT

Objectives: To explore the optimal choice of seven diffusion models (DWI, IVIM, DKI, CTRW, FROC, SEM, and sADC) to assess renal interstitial fibrosis (IF) and annual renal function loss in chronic kidney disease (CKD).

Methods: One hundred thirty-three CKD patients and 30 controls underwent multi-b diffusion sequence scans. Patients were divided into the training, testing, and temporal external validation sets. Least absolute shrinkage and selection operator regression and logistic regression were used to select the optimal metrics for distinguishing the mild from moderate-to-severe IF. The performances of imaging, clinical, and combined models were compared. A linear mixed-effects model calculated estimated glomerular filtration rate (eGFR) slope, and multiple linear regression assessed the association between metrics and 1–3-year eGFR slopes.

Results: The training, testing, and temporal external validation sets had 75, 30, and 28 patients, respectively. The combined model incorporating cortical f_{IVIM} , MK_{DKI} and eGFR was superior to the clinical model combining the eGFR and 24-hour urinary protein in all sets (net reclassification index [NRI] > 0, $p < 0.05$). Decision curve analysis showed the combined model provided greater net clinical benefit across most thresholds. Fifty-two, 35, and 16 patients completed 1-, 2-, and 3-year follow-ups. After adjusting for covariates, cortical f_{IVIM} correlated with the 1-year eGFR slope ($\beta = 30.600$, $p = 0.001$), and cortical α_{SEM} correlated with the 2- and 3-year eGFR slopes ($\beta = 44.859$, $p = 0.002$; $\beta = 95.631$, $p = 0.019$).

Conclusions: A combined model of cortical f_{IVIM} , MK_{DKI} and eGFR provides a useful comprehensive tool for grading IF, with cortical f_{IVIM} and α_{SEM} as potential biomarkers for CKD progression.

ARTICLE HISTORY

Received 27 December 2024

Revised 7 March 2025

Accepted 12 March 2025

KEYWORDS





Diffusion weighted imaging; chronic kidney disease; interstitial fibrosis; progression


Introduction

Chronic kidney disease (CKD) is marked by a gradual decline in renal function, potentially developing into renal failure, which poses a substantial clinical and economic burden on healthcare systems worldwide [1]. Renal interstitial fibrosis (IF) is a key pathological feature of CKD [2], and its accurate assessment is crucial for guiding clinical decision-making. While renal biopsy is the most commonly used method for evaluating IF in clinical, it is invasive. Besides, CKD progression can vary greatly among patients. Early identification of patients

with rapid progression, followed by proactive interventions and close monitoring, can help prevent poor outcomes [3]. Therefore, exploring noninvasive and reliable biomarkers for grading IF and predicting CKD progression is of great value.

Functional magnetic resonance imaging (MRI) can be a valuable diagnostic tool due to its ability to visualize renal pathophysiological processes. Diffusion weighted imaging (DWI) stands out as the most widely used functional MRI sequence in clinical practice. By employing multiple b-values and applying diverse computational models, DWI can provide rich microstructural information from multiple

CONTACT Min Han  minhan@tjh.tjmu.edu.cn  Department of Nephrology, Tongji Hospital, Tongji Medical College, Huazhong University of Science and Technology, 1095 Jiefang Avenue, Wuhan 430030, Hubei, China; Zhen Li  zhenli@hust.edu.cn  Department of Radiology, Tongji Hospital, Tongji Medical College, Huazhong University of Science and Technology, 1095 Jiefang Avenue, Wuhan 430030, Hubei, China.

 Supplemental data for this article can be accessed online at <https://doi.org/10.1080/0886022X.2025.2480751>.

© 2025 The Author(s). Published by Informa UK Limited, trading as Taylor & Francis Group.

This is an Open Access article distributed under the terms of the Creative Commons Attribution-NonCommercial License (<http://creativecommons.org/licenses/by-nc/4.0/>), which permits unrestricted non-commercial use, distribution, and reproduction in any medium, provided the original work is properly cited. The terms on which this article has been published allow the posting of the Accepted Manuscript in a repository by the author(s) or with their consent.

perspectives. For instance, the apparent diffusion coefficient (ADC), derived from the proposed mono-exponential model, depicts the apparent diffusion of water molecules. Intravoxel incoherent motion (IVIM)-DWI applies a bi-exponential model and enables assessing microcirculatory perfusion [4]. Non-Gaussian models, including diffusion kurtosis imaging (DKI), the stretched exponential model (SEM), fractional order calculus (FROC), and continuous-time random-walk (CTRW), can detect microstructural heterogeneity [5–7]. The shifted ADC (sADC) derived from the DWI-based virtual MR elastography (MRE) can be converted into a measure of tissue stiffness [8–11]. Despite the availability of these models, few studies have systematically assessed their performance and which model metrics contribute the most in IF grading remains unclear. Besides, the estimated glomerular filtration rate (eGFR) slope is a reliable surrogate endpoint for CKD progression [12]. The association between diffusion metrics and the eGFR slope has not yet been extensively studied.

This study aims to evaluate the performance of seven diffusion models in grading renal IF, identify the most valuable diffusion metrics, and integrate them with clinical variables to develop a comprehensive and noninvasive tool for renal IF evaluation. Additionally, we will explore the relationship between all diffusion metrics and the 1-, 2-, and 3-year eGFR

slopes to identify potential imaging biomarkers for predicting CKD progression, thereby improving risk stratification and patient outcomes.

Materials and methods

Ethics approval

This study was conducted in accordance with the ethical principles of the Declaration of Helsinki and was approved by the Ethics Committee of our hospital (TJ-IRB202406070). Written informed consent was obtained from all participants. All collected data were anonymized and securely stored to ensure the protection of participants' privacy.

Study population

From January 2021 to April 2024, we retrospectively collected data from 265 CKD patients from the Department of Nephrology. One hundred and thirty-two patients were excluded (Figure 1). Finally, 133 patients (67 women, median age: 41 years) were included in the analysis. One hundred five patients collected from January 2021 to September 2023 were divided into the training ($n=75$) or testing ($n=30$) set

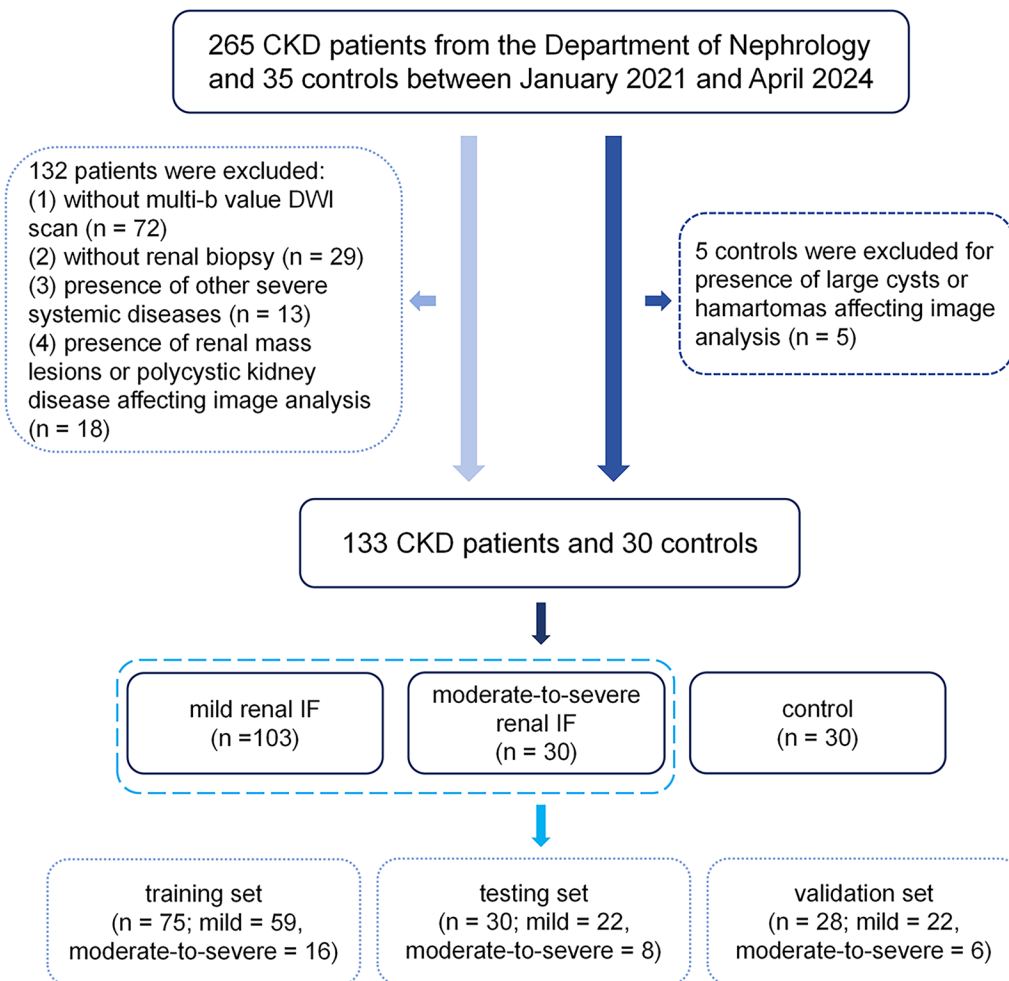


Figure 1. Flowchart of the study population. CKD, chronic kidney disease; DWI, diffusion-weighted imaging; IF, interstitial fibrosis.

at a 7:3 ratio. Twenty-eight patients collected from October 2023 to April 2024 were used as the temporal external validation set. Besides, a total of 35 patients admitted in the same period due to other reasons such as lumbar disk herniation, anxiety, and depression, who had undergone renal multi b-value DWI scans, were selected as the control group. They had normal renal function and urinalysis tests, and had no history of urinary system disease, systemic metabolic or endocrine diseases, and vascular diseases. Five controls were excluded due to the presence of large cysts or hamartomas, and finally 30 healthy controls (14 women, median age: 38years) were included.

MRI acquisition

All participants underwent renal MRI on a 3T-MRI scanner (MAGNETOM Skyra, Siemens Healthcare, Erlangen, Germany) with an 18-channel body array coil. The sequences include T1-weighted imaging (T1WI), T2-weighted imaging (T2WI), and ZOOMit multi-b DWI. The axial multi-b DWI was performed with the following parameters: repetition time, 7700ms; echo time, 71ms; matrix size, 120×120; eleven b values including 0, 20, 50, 80, 100, 200, 500, 800, 1000, 1500, 2000s/mm²; scan time, 10min 16s. The average was taken for the four trace scan directions, and the diffusion anisotropy was ignored. The specific parameters are shown in [Table S1](#).

Image analysis

The parametric maps of various DWI models were calculated using an in-house software prototype developed by MR Station (Chengdu Zhongying Medical Technology Co., Ltd., Chengdu, Sichuan, China). The specific formulas, applied b values, and calculated diffusion metrics are shown in the [Supplementary Materials](#).

Two radiologists with 5 and 8years each of abdominal MRI experience reviewed all the images. They manually selected three central axial planes near the kidney hilum on the images of b=0s/mm² and drew the region of interest (ROI). Taking the T2WI images as a reference, six cortical ROIs followed the outline of the kidney, and 12–18 medullary ROIs were delineated in the middle of the renal parenchyma ([Figure 2](#)). The cortical and medullary diffusion metrics were calculated from the separate averages of the cortical and medullary ROIs.

Clinicopathological information

Patients' clinicopathological information was extracted from electronic medical records. Serum creatinine levels at admission were recorded, and eGFR was calculated using the Chronic Kidney Disease Epidemiology Collaboration formula [13]. All patients underwent renal biopsy, and the pathological evaluation was performed by a nephrologist with over 15years of clinical experience.

A semiquantitative method was used to assess IF based on the percentage of IF lesions in the sampled tissue area: one point was defined as ≤25% = mild IF, two points as 26%–50% = moderate IF, and three points as >50% = severe IF.

eGFR slope calculation

The eGFR recorded at patient admission served as the baseline value, with subsequent measurements taken during hospitalizations or outpatient follow-ups until April 1, 2024. The 1-year eGFR slope was determined for patients at two specific times: baseline and 1 year ± 3 months from baseline as previously described [14,15]. Similarly, the 2- and 3-year eGFR slopes were also calculated. Patients were required to have at least three eGFR readings within these specified intervals.

Statistical analysis

Statistical analysis was conducted using SPSS (version 25.0), R software (version 3.6.3), and MedCalc (version 15.8). All tests were two-tailed with a significance threshold of $p < 0.05$. Interobserver repeatability was assessed using the intraclass correlation coefficient (ICC). Continuous variables were analyzed with independent-sample t-tests or Mann-Whitney U tests, while categorical variables were evaluated using chi-square tests. Diffusion metrics across control, mild, and moderate-to-severe renal IF groups were compared using either one-way analysis of variance with Tukey's post hoc test or the Kruskal-Wallis test, with Bonferroni correction for multiple comparisons ($p < 0.05/3$). Partial correlation analysis, adjusted for age, assessed correlations between diffusion metrics and renal IF score, with a Bonferroni-adjusted significance level of $p < 0.05/30$.

In the training set, diffusion metrics with significant differences between mild and moderate-to-severe renal IF groups were selected for least absolute shrinkage and selection operator (LASSO) regression. Z-score normalization was applied to eliminate dimensional differences. Diffusion metrics with non-zero coefficients identified through LASSO regression under the lambda.min condition were subsequently subjected to multivariate logistic regression analysis. Metrics with a significance level of $p < 0.05$ in the multivariate logistic regression were identified as the most valuable and were subsequently used to construct the imaging model. Clinical indicators with significant differences between two groups were included in multivariate logistic regression analysis to establish the clinical model. Besides, a combined model was built based on the selected diffusion and clinical parameters. The performance of the models was evaluated using receiver operating characteristic (ROC) curves and the area under the curve (AUC), with the Delong test applied to compare AUC values. To further assess the incremental predictive value, reclassification analysis was performed, quantified by the net reclassification index (NRI) and the integrated discrimination index (IDI). An NRI > 0 and IDI > 0 suggest that the new model improves risk reclassification and

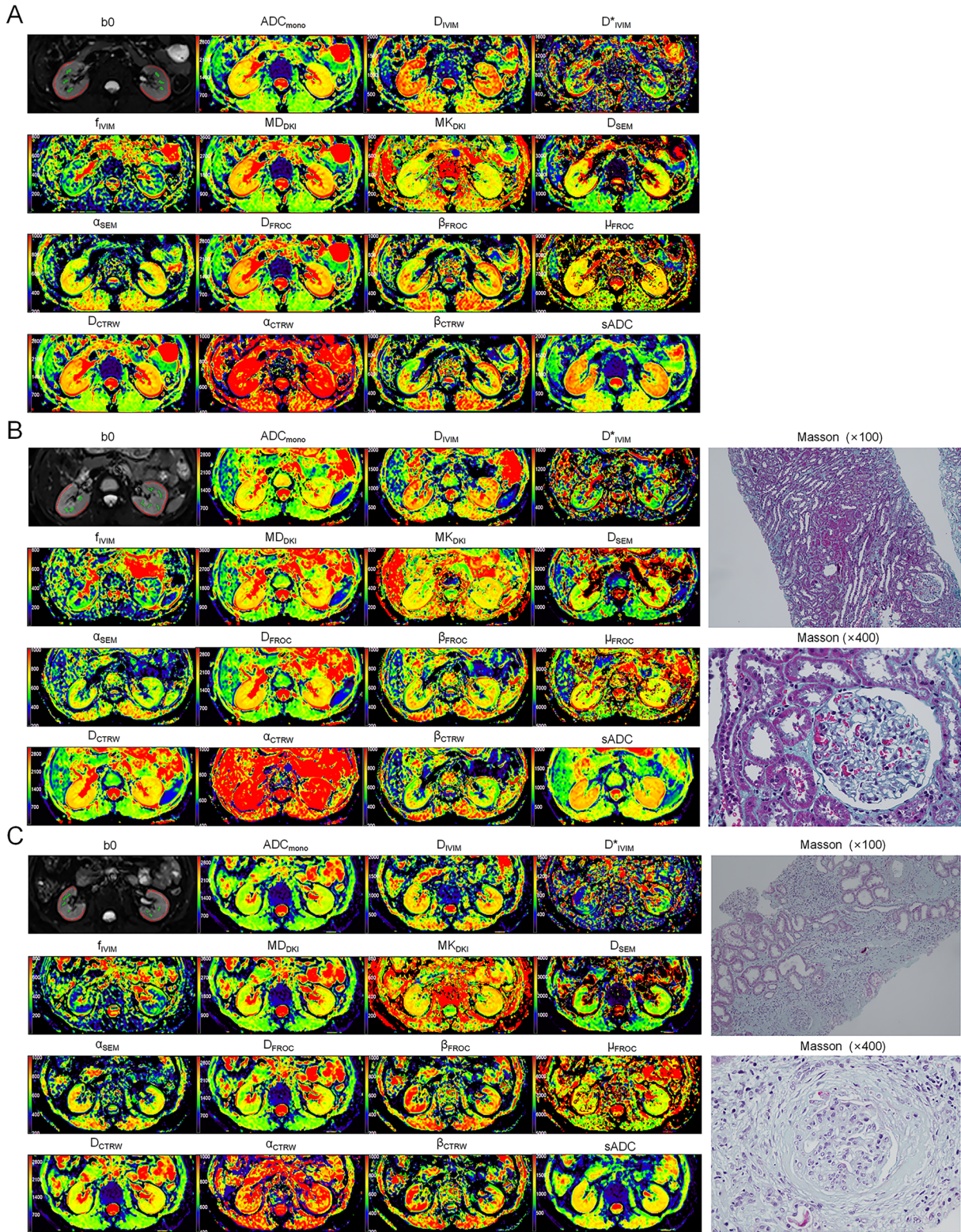


Figure 2. Maps of ROI, DWI model metrics, and pathology. A) 24-year-old female volunteer (control), eGFR = 121.7 mL/min/1.73m²; B) 29-year-old female CKD patient, eGFR = 111.8 mL/min/1.73m², immunoglobulin A nephropathy, renal IF score 1; C) 45-year-old male CKD patient, eGFR = 32.5 mL/min/1.73m², immunoglobulin A nephropathy, renal IF score 2. ROI, region of interest; CKD, chronic kidney disease; eGFR, estimated glomerular filtration rate; ADC_{mono}, apparent diffusion coefficient from Mono-exponential model; IVIM, intravoxel incoherent motion; D_{IVIM}, true diffusion coefficient from IVIM model; D*_{IVIM}, pseudo-diffusion coefficient from IVIM model; f_{IVIM}, perfusion fraction from IVIM model; DKI, diffusion kurtosis imaging; MD_{DKI}, mean diffusivity from DKI model; MK_{DKI}, mean kurtosis from DKI model; SEM, stretched exponential model; DDC_{SEM}, distributed diffusion coefficient from SEM; α_{SEM}, intravoxel heterogeneity index from SEM; FROC, fractional order calculus; D_{FROC}, diffusion coefficient from FROC model; β_{FROC}, fractional order parameter from FROC model; μ_{FROC}, microstructural quantity from FROC model; CTRW, continuous-time random-walk; D_{CTRW}, anomalous diffusion coefficient from CTRW model; α_{CTRW}, temporal diffusion heterogeneity index from CTRW model; β_{CTRW}, spatial diffusion heterogeneity index from CTRW model; sADC, shift apparent diffusion coefficient.

enhances discrimination between groups compared to the baseline model. Additionally, decision curve analysis (DCA) was conducted to evaluate the clinical utility of the models.

The mixed-effects model calculated patient-specific 1-, 2-, and 3-year eGFR slopes, using eGFR as the dependent variable and time of measurement as the independent variable. Pearson or Spearman correlations assessed the relationships between diffusion metrics and eGFR slopes, applying a Bonferroni-adjusted significance level of $p < 0.05/30$. If significant correlations were found, further multiple linear regression analysis was conducted.

Results

Participants' characteristics

There were no significant differences in sex and age between the patient and control groups ($p = 0.714$; $p = 0.223$; Table 1). The mild and moderate-to-severe renal IF groups included 103 (77.4%) and 30 (22.6%) patients, respectively.

Comparisons of diffusion metrics

The ICCs of all diffusion metrics were greater than 0.750 (Table S2). Table 2 and Figure 3 show the between-group differences. The renal parenchymal ADC_{mono} , D_{IVIM} , MD_{DKI} , MK_{DKI} , DDC_{SEM} , D_{FROC} , μ_{FROC} , D_{CTRW} , and sADC and cortical D^* , f_{IVIM} , and α_{CTRW} differed significantly across the control, mild, and moderate-to-severe groups (all $p < 0.05$). Excluding the renal parenchymal D^* , α_{SEM} , β_{FROC} , and β_{CTRW} and medullary f_{IVIM} , MK_{DKI} and α_{CTRW} , all other metrics differed significantly between the mild and moderate-to-severe groups (all $p < 0.05/3$).

Correlations between diffusion metrics and renal IF score

The cortical ADC_{mono} , f_{IVIM} , MD_{DKI} , MK_{DKI} , DDC_{SEM} , D_{FROC} , μ_{FROC} , D_{CTRW} , α_{CTRW} , and sADC and medullary ADC_{mono} , MD_{DKI} , DDC_{SEM} , D_{FROC} , D_{CTRW} , and sADC were significantly correlated with renal IF score (all $p < 0.05/30$). The specific correlation coefficient and p value are displayed in Table 3.

LASSO regression analysis and imaging model development

Table S3 shows the characteristics of the patients in the training, testing, and validation sets. The training, testing, and validation sets did not differ significantly in any variables (all $p > 0.05$).

In the training set, 20 diffusion metrics differed significantly between the mild and moderate-to-severe renal IF groups (all $p < 0.05$; Table S4). In LASSO regression analysis, when lambda was 0.028 (Log lambda = -3.577), the cortical f_{IVIM} , MK_{DKI} , DDC_{SEM} , and α_{CTRW} and medullary sADC were screened out (Figure 4). After multivariate logistic regression, only cortical f_{IVIM} (odds ratio [OR]: 0.079, 95% confidence interval [95%CI]: 0.012–0.519, $p = 0.008$) and MK_{DKI} (OR: 21.940, 95%CI: 3.272–147.110, $p = 0.001$) were statistically

Table 1. Characteristics of all participants.

Characteristic	Patients (n = 133)	Volunteers (n = 30)	p-value
Male/Female, n (%)	66 (49.6%)/ 67 (50.4%)	16 (53.3%)/ 14 (46.7%)	0.714
Age (years)	41 (32–53)	38 (28–51)	0.223
eGFR (mL/min/1.73 m ²)	74.0 ± 33.0	114.8 ± 11.2	<0.001***
CKD stage		/	/
CKD 1–2	85 (63.9%)		
CKD 3–5	48 (36.1%)		
Pathological type		/	/
IgA nephropathy	66 (49.6%)		
Membranous nephropathy	21 (15.8%)		
Focal segmental glomerulosclerosis	19 (14.3%)		
Minimal change nephropathy	7 (5.3%)		
Henoch-Schonlein nephritis	5 (3.8%)		
Diabetic nephropathy	4 (3.0%)		
Hypertension nephropathy	4 (3.0%)		
Lupus nephritis	4 (3.0%)		
Hepatitis B virus associated nephropathy	1 (0.8%)		
ANCA-associated glomerulonephritis	1 (0.8%)		
Alport syndrome	1 (0.8%)		
Renal IF		/	/
Mild (≤25%)	103 (77.4%)		
Moderate (26 ~ 50%)	23 (17.3%)		
Severe (>50%)	7 (5.3%)		

*** $p < 0.001$; eGFR, estimated glomerular filtration rate; CKD, chronic kidney disease; IgA, immunoglobulin A; ANCA, anti-neutrophil cytoplasmic antibody; IF, interstitial fibrosis.

significant (Table 4). The imaging model was developed based on these two metrics.

Clinical model establishment and combined model building

In the training set, hemoglobin, eGFR, and 24-h urinary protein differed significantly between the mild and moderate-to-severe renal IF groups (131 vs. 108, $p = 0.042$; 81.5 vs. 39.1, $p < 0.001$; 818.75 vs. 2309.95, $p = 0.006$, respectively; Table S4). After multiple logistic regression, eGFR (OR: 0.093, 95%CI: 0.026–0.340, $p < 0.001$) and 24-h urinary protein (OR: 2.470, 95%CI: 1.038–5.878, $p = 0.041$) were selected to establish the clinical model (Table 4).

The cortical f_{IVIM} (OR: 0.088, 95%CI: 0.010–0.754, $p = 0.027$), MK_{DKI} (OR: 16.850, 95%CI: 1.727–164.368, $p = 0.015$), and eGFR (OR: 0.260, 95%CI: 0.069–0.986, $p = 0.048$) were used to build the combined model (Table 4).

Diagnostic performances for distinguishing mild from moderate-to-severe renal IF

Table 5 and Figure 5 show the diagnostic performances of all models for distinguishing between mild and moderate-to-severe renal IF in all sets. The imaging model had AUCs of 0.944, 0.898, and 0.886 in the training, testing, and validation sets, respectively. Although DeLong's test revealed no significant differences, the combined model consistently demonstrated higher AUCs than did the clinical model in the training (0.961 vs. 0.915, $p = 0.138$), testing (0.932 vs. 0.869, $p = 0.356$), and validation (0.917 vs. 0.841, $p = 0.225$) sets. The

Table 2. Comparisons of diffusion metrics across the control, mild, and moderate-to-severe renal interstitial fibrosis groups.

Metric	Control (n = 30)	Mild IF (n = 103)	Moderate-to-severe IF (n = 30)	p-value	p ^a -value	p ^b -value	p ^v -value
Cortical							
ADC _{mono}	2.185 ± 0.112	2.071 ± 0.149	1.860 ± 0.174	<0.001***	0.001**	<0.001***	<0.001***
D _{IVIM}	1.542 ± 0.156	1.515 ± 0.160	1.409 ± 0.128	0.001**	0.675	0.003**	0.003**
D* _{IVIM}	0.904 (0.809, 1.013)	0.814 (0.743, 0.961)	0.789 (0.697, 0.866)	0.004**	0.032	0.045	0.001**
f _{IVIM}	0.361 (0.340, 0.436)	0.371 (0.336, 0.394)	0.300 (0.279, 0.329)	<0.001***	0.212	<0.001***	<0.001***
MD _{DKI}	2.935 (2.871, 3.170)	2.781 (2.615, 2.942)	2.463 (2.328, 2.463)	<0.001***	0.001**	<0.001***	<0.001***
MK _{DKI}	0.499 ± 0.024	0.521 ± 0.028	0.566 ± 0.028	<0.001***	<0.001***	<0.001***	<0.001***
DDC _{SEM}	3.019 ± 0.227	2.905 ± 0.280	2.552 ± 0.285	<0.001***	0.110	<0.001***	<0.001***
α _{SEM}	0.636 ± 0.053	0.647 ± 0.040	0.645 ± 0.061	0.530	0.498	0.964	0.764
D _{FROC}	2.525 ± 0.199	2.374 ± 0.243	2.068 ± 0.221	<0.001***	0.005**	<0.001***	<0.001***
β _{FROC}	0.710 ± 0.052	0.728 ± 0.042	0.738 ± 0.060	0.076	0.187	0.559	0.068
μ _{FROC}	7.745 ± 0.223	7.683 ± 0.241	7.410 ± 0.173	<0.001***	0.386	<0.001***	<0.001***
D _{CTRW}	2.480 ± 0.148	2.341 ± 0.211	2.063 ± 0.215	<0.001***	0.003**	<0.001***	<0.001***
α _{CTRW}	0.979 (0.969, 0.986)	0.975 (0.962, 0.985)	0.967 (0.944, 0.979)	0.011*	0.234	0.016*	0.004**
β _{CTRW}	0.653 ± 0.060	0.679 ± 0.052	0.683 ± 0.064	0.067	0.080	0.923	0.104
sADC	1.567 ± 0.060	1.487 ± 0.098	1.378 ± 0.088	<0.001***	<0.001***	<0.001***	<0.001***
Medullary							
ADC _{mono}	1.779 (1.722, 1.813)	1.715 (1.661, 1.826)	1.617 (1.571, 1.680)	<0.001***	0.052	<0.001***	<0.001***
D _{IVIM}	1.410 ± 0.076	1.396 ± 0.100	1.333 ± 0.117	0.005**	0.767	0.008**	0.009**
D* _{IVIM}	0.506 ± 0.142	0.523 ± 0.130	0.551 ± 0.140	0.429	0.813	0.588	0.407
f _{IVIM}	0.260 ± 0.031	0.258 ± 0.047	0.238 ± 0.047	0.078	0.961	0.085	0.132
MD _{DKI}	2.302 ± 0.106	2.253 ± 0.187	2.087 ± 0.186	<0.001***	0.367	<0.001***	<0.001***
MK _{DKI}	0.515 ± 0.019	0.546 ± 0.033	0.562 ± 0.033	<0.001***	<0.001***	0.034	<0.001***
DDC _{SEM}	2.241 ± 0.141	2.204 ± 0.247	1.969 ± 0.240	<0.001***	0.714	<0.001***	<0.001***
α _{SEM}	0.661 ± 0.019	0.651 ± 0.039	0.660 ± 0.047	0.267	0.368	0.457	0.991
D _{FROC}	1.796 ± 0.115	1.782 ± 0.166	1.658 ± 0.143	<0.001***	0.904	<0.001***	0.002**
β _{FROC}	0.877 (0.850, 0.899)	0.868 (0.838, 0.897)	0.872 (0.842, 0.889)	0.716	0.518	0.848	0.359
μ _{FROC}	7.543 ± 0.290	7.439 ± 0.275	7.271 ± 0.288	0.001**	0.172	0.013*	0.001**
D _{CTRW}	1.934 ± 0.086	1.898 ± 0.146	1.770 ± 0.141	<0.001***	0.400	<0.001***	<0.001***
α _{CTRW}	0.848 ± 0.047	0.860 ± 0.055	0.851 ± 0.049	0.484	0.535	0.711	0.972
β _{CTRW}	0.860 (0.828, 0.860)	0.858 (0.821, 0.893)	0.856 (0.828, 0.890)	0.996	0.923	0.991	0.965
sADC	1.456 (1.415, 1.491)	1.393 (1.354, 1.449)	1.282 (1.245, 1.339)	<0.001***	0.001**	<0.001***	<0.001***

p: comparison across control, mild, and moderate-to-severe groups; p^a: comparison between control and mild groups; p^b: comparison between mild and moderate-to-severe groups; p^v: comparison between control and moderate-to-severe groups. Variables marked with an asterisk indicate p^{a/b/v} < 0.05/3, *p < 0.05, **p < 0.01, and ***p < 0.001. IF, interstitial fibrosis; ADC_{mono}, apparent diffusion coefficient from mono-exponential model; IVIM, intravoxel incoherent motion; D_{IVIM}, true diffusion coefficient from IVIM model; D*_{IVIM}, pseudo-diffusion coefficient from IVIM model; f_{IVIM}, perfusion fraction from IVIM model; DKI, diffusion kurtosis imaging; MD_{DKI}, mean diffusivity from DKI model; MK_{DKI}, mean kurtosis from DKI model; SEM, stretched exponential model; DDC_{SEM}, distributed diffusion coefficient from SEM; α_{SEM}, intravoxel heterogeneity index from SEM; FROC, fractional order calculus; D_{FROC}, diffusion coefficient from FROC model; β_{FROC}, fractional order parameter from FROC model; μ_{FROC}, microstructural quantity from FROC model; CTRW, continuous-time random-walk; D_{CTRW}, anomalous diffusion coefficient from CTRW model; α_{CTRW}, temporal diffusion heterogeneity index from CTRW model; β_{CTRW}, spatial diffusion heterogeneity index from CTRW model; sADC, shift apparent diffusion coefficient.

continuous NRI showed a statistically significant improvement across the training (NRI = 1.104, p < 0.001), testing (NRI = 1.227, p < 0.001), and validation (NRI = 0.970, p = 0.021) sets. DCA indicated that in all sets, the combined model offered a greater net clinical benefit than did the clinical model over most threshold probabilities.

Associations between diffusion metrics and eGFR slope

Fifty-two, 35, and 16 patients met the calculation criteria for the 1-, 2-, and 3-year eGFR slopes, respectively. The median follow-up times for the 1-, 2-, and 3-year analyses were 14.4, 25.2, and 34.2 months, respectively, and the median numbers of eGFR measurements were 10, 15, and 18, respectively. The mean slopes for the 1-, 2-, and 3-year intervals were 1.675, −0.160, and −0.337 mL/min/1.73 m² per year, respectively.

The cortical f_{IVIM} was significantly correlated with the 1-year eGFR slope (r = 0.442, p = 0.001) (Figure 6). The cortical α_{SEM} was significantly correlated with the 2-year (r = 0.557, p = 0.001) and 3-year (r = 0.732, p = 0.001) eGFR slopes. In the multivariate linear regression analyses, when adjusted for

age, sex, primary/secondary, angiotensin-converting enzyme inhibitor/angiotensin receptor blocker use, immunosuppressant use, baseline eGFR, mean arterial pressure, 24-h urinary protein (ln-transformed), and renal IF score, the cortical f_{IVIM} correlated positively with the 1-year eGFR slope (β = 30.600, 95%CI: 13.658–47.541, p = 0.001; Table 6), and the cortical α_{SEM} correlated positively with the 2-year eGFR slope (β = 44.859, 95%CI: 17.610–72.108, p = 0.002) and 3-year eGFR slope (β = 95.631, 95%CI: 26.299–164.964, p = 0.019).

Discussion

In this study, we explored the value of seven diffusion models in evaluating renal IF and found that the cortical f_{IVIM} and MK_{DKI} were the most valuable diffusion metrics for distinguishing mild from moderate-to-severe renal IF. The model combining cortical f_{IVIM}, MK_{DKI}, and eGFR demonstrated improved diagnostic performance compared to the clinical model based on eGFR and 24-h urinary protein. Additionally, the cortical f_{IVIM} was associated with 1-year eGFR loss, and cortical α_{SEM} was associated with 2- and 3-year eGFR losses,

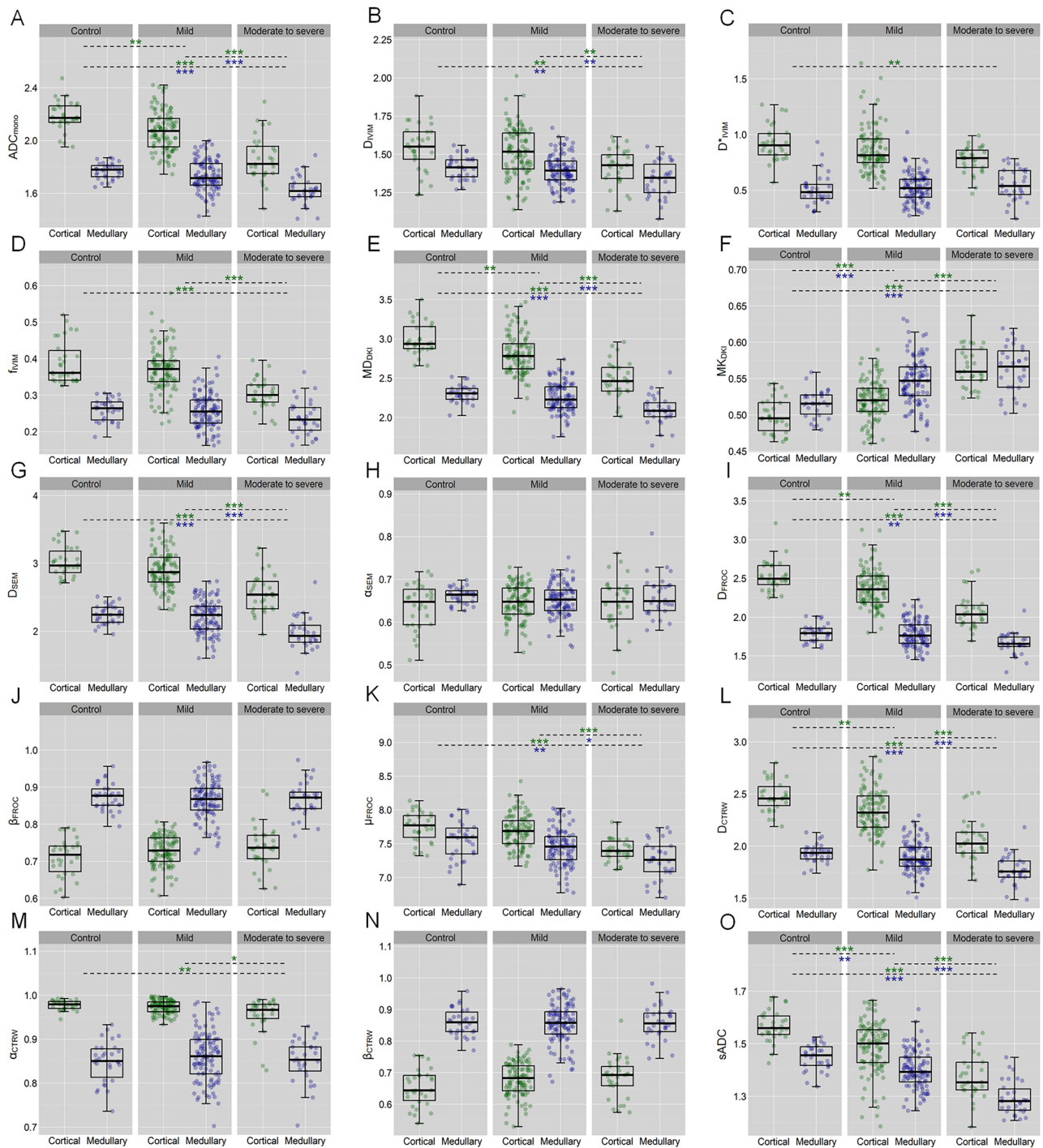


Figure 3. Comparisons of diffusion metrics across control, mild, and moderate-to-severe renal interstitial fibrosis groups. Green asterisks above the dashed lines indicate differences in cortical parameters between groups; purple asterisks below the dashed lines indicate differences in medullary parameters between groups. Only group differences with $p < 0.05/3$ are shown, * $p < 0.05$, ** $p < 0.01$, and *** $p < 0.001$.

suggesting their potential as noninvasive imaging biomarkers for predicting short-term CKD progression.

f_{IVIM} is related to the fraction volume of capillary blood flow. In our study, the cortical f_{IVIM} showed significant correlation with IF score and emerged as one of the most valuable diffusion metrics for differentiating mild from moderate-to-severe IF. This is likely due to its sensitivity to capillary loss and hypoperfusion, which are key features of fibrotic kidneys and drivers of further fibrosis-related damage [16]. D^*_{IVIM} and f_{IVIM}

are both perfusion-related metrics. However, our results showed no significant difference in D^*_{IVIM} between the mild and moderate-to-severe IF groups, nor did D^*_{IVIM} correlate significantly with IF score. The possible explanation is that the instability in the fitting of D^*_{IVIM} limits its clinical applicability [17–19]. Cortical MK_{DKI} is another key metric that can characterize tissue heterogeneity. It increased as the IF score increased. Higher kurtosis values indicate greater hindrance and restriction to normal diffusion. As fibrotic tissue

gradually replaces normal tissue, increased collagen deposition creates more diffusion barriers, leading to more restricted water molecule diffusion. Although α_{SEM} , like MK_{DKI} , represents deviation from a mono-exponential distribution, it was not significantly correlated with histopathological assessment of fibrosis in this study, which is consistent with previous research [20,21]. These two metrics are not completely

Table 3. Partial correlation analysis between diffusion metrics and renal interstitial fibrosis score.

Metric	Cortical		Medullary	
	r	p-value	r	p-value
ADC _{mono}	-0.482	<0.001***	-0.394	<0.001***
D _{IVIM}	-0.254	0.003	-0.224	0.010
D* _{IVIM}	-0.203	0.020	0.042	0.636
f _{IVIM}	-0.424	<0.001***	-0.179	0.040
MD _{DKI}	-0.458	<0.001***	-0.373	<0.001***
MK _{DKI}	0.558	<0.001***	0.170	0.051
DDC _{SEM}	-0.450	<0.001***	-0.386	<0.001***
α_{SEM}	-0.059	0.498	0.049	0.578
D _{FROC}	-0.442	<0.001***	-0.318	<0.001***
β_{FROC}	0.030	0.730	-0.029	0.742
μ_{FROC}	-0.409	<0.001***	-0.229	0.008
D _{CTRW}	-0.450	<0.001***	-0.373	<0.001***
α_{CTRW}	-0.318	<0.001***	-0.046	0.597
β_{CTRW}	0.006	0.193	-0.012	0.889
sADC	-0.408	<0.001***	-0.533	<0.001***

Variables marked with an asterisk indicate $p < 0.05/30$; *** $p < 0.001$.

consistent in evaluating pathophysiological states, and one study found that although α_{SEM} has limited value in evaluating IF, it is associated with the active inflammatory state in patients with lupus nephritis [22].

We also evaluated the performance of advanced diffusion models including FROC and CTRW in assessing renal IF. Our results demonstrated that renal parenchymal D_{FROC} and D_{CTRW} values, as well as cortical μ_{FROC} and α_{CTRW} values, were significantly lower in the moderate-to-severe fibrosis group compared to the mild fibrosis group, and these metrics exhibited significant correlations with IF score. D_{FROC} and D_{CTRW} quantify the diffusion of water molecules, μ_{FROC} reflects microenvironmental complexity, and α_{CTRW} represents temporal heterogeneity [6,23]. As tissue heterogeneity increases, the free diffusion of water molecules becomes more hindered or restricted, leading to greater variations in the mean free path and inconsistent waiting times for the next diffusion movement [24,25]. Consequently, D_{FROC} , D_{CTRW} , μ_{FROC} , and α_{CTRW} values decrease. However, after applying LASSO and multivariate logistic regression analyses, these parameters lost their significance. While advanced models provide valuable insights into tissue microstructure, their clinical applicability remains a crucial consideration [26]. Our current results verified that in evaluating renal IF, the priority of fitting these high-order diffusion models is ranked after IVIM and DKI models.

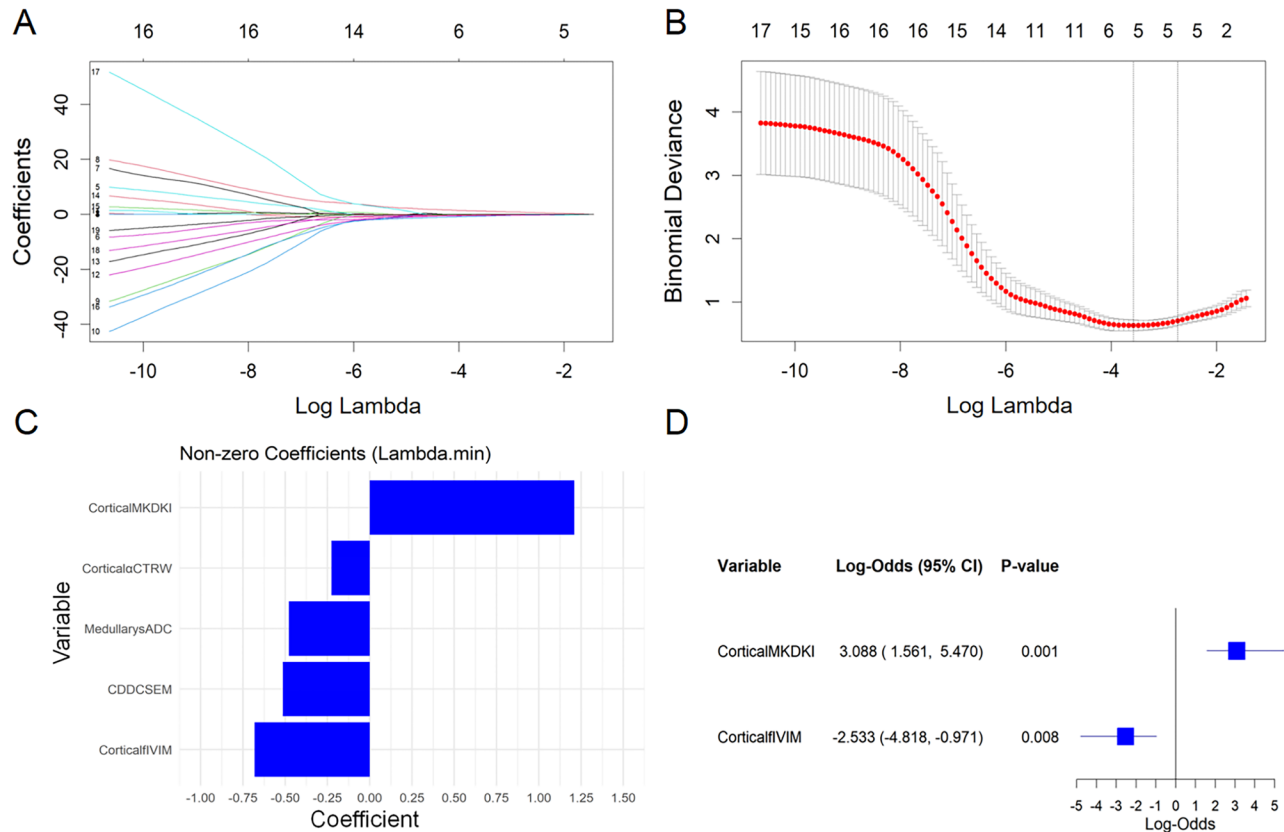


Figure 4. Least absolute shrinkage and selection operator and logistic regression analysis of diffusion metrics. (A) Coefficient paths as the regularization strength (log lambda) change. (B) Cross-validation curve. The left vertical line represents the lambda.min value that minimizes the model deviance; the right vertical line represents the lambda.1se value, which is the most parsimonious model within one standard error of the minimum deviance. (C) Coefficient distribution. When the lambda.min value was set as 0.028 (log lambda = -3.577), the cortical f_{IVIM} , MK_{DKI} , DDC_{SEM} , α_{CTRW} and medullary sADC were screened out. (D) Forest plot. After logistic regression, the cortical f_{IVIM} and MK_{DKI} were statistically significant.

Table 4. Multivariate logistic regression analysis for distinguishing mild from moderate-to-severe renal interstitial fibrosis in the training set.

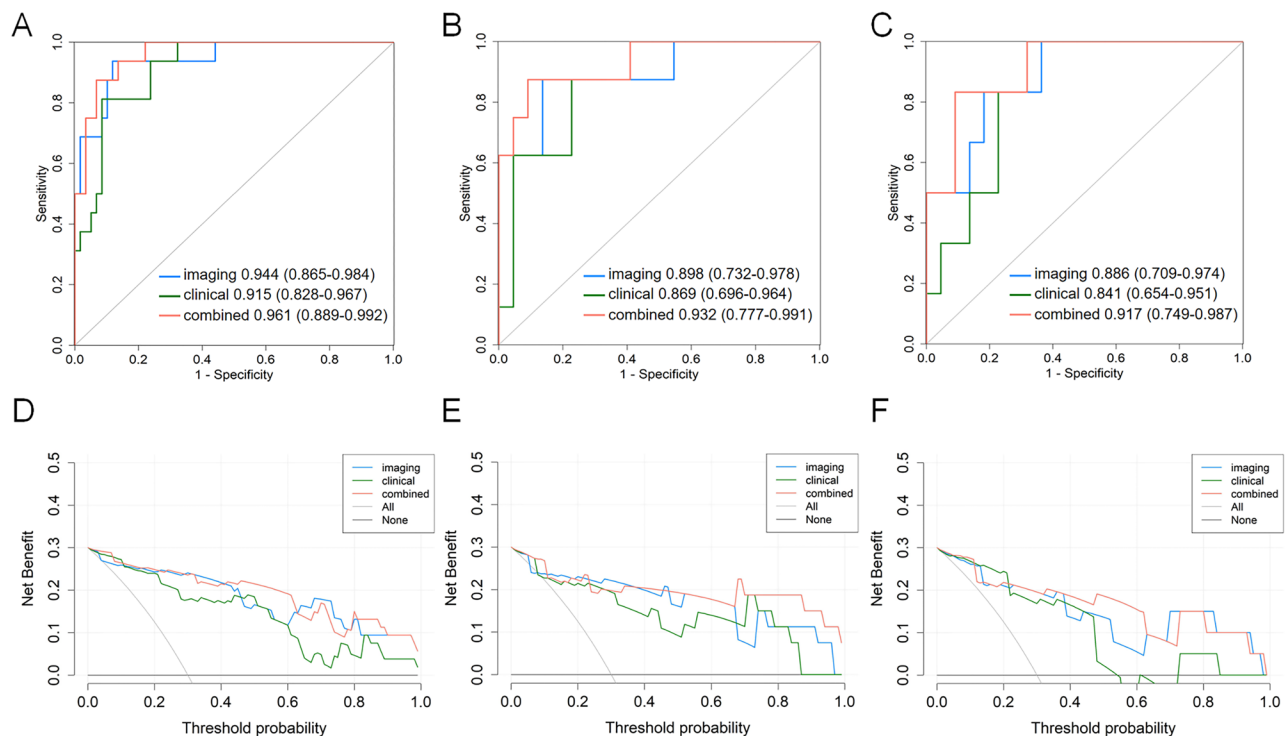
Variable	Multicollinearity diagnosis		Multivariate analysis			
	VIF	β	SD	Wald	OR (95% CI)	p-value
Diffusion metrics						
Cortical α_{CTRW}	1.181					
Cortical DDC _{SEM}	1.947					
Cortical MK _{DKI}	1.732	3.088	0.971	10.119	21.940 (3.272–147.110)	0.001**
Cortical f_{IVIM}	1.428	−2.533	0.958	6.999	0.079 (0.012–0.519)	0.008**
Medullary sADC	1.995					
Clinical indicators						
hemoglobin (g/L)	1.076					
eGFR (mL/min/1.73 m ²)	1.096	−2.371	0.659	12.940	0.093 (0.026–0.340)	<0.001***
24-hour urinary protein (mg/24h)	1.050	0.904	0.442	4.177	2.470 (1.038–5.878)	0.041*
Combined variables						
Cortical α_{CTRW}	1.301					
Cortical DDC _{SEM}	1.996					
Cortical MK _{DKI}	1.906	2.824	1.162	5.906	16.850 (1.727–164.368)	0.015*
Cortical f_{IVIM}	1.728	−2.426	1.094	4.919	0.088 (0.010–0.754)	0.027*
Medullary sADC	2.254					
hemoglobin (g/L)	1.256					
eGFR (mL/min/1.73 m ²)	2.057	−1.347	0.680	3.926	0.260 (0.069–0.986)	0.048*
24-hour urinary protein (mg/24h)	1.262					

* $p < 0.05$, ** $p < 0.01$, and *** $p < 0.001$. VIF, variance inflation factor; SD, standard deviation; OR, odds ratio; CI, confidence interval; eGFR, estimated glomerular filtration rate.

Table 5. Diagnostic performances of models for distinguishing the mild from moderate-to-severe renal interstitial fibrosis groups.

Set	Model	AUC (95% CI)	p^a -value	Sensitivity	Specificity	Accuracy	F1_score	continuous NRI	p^b -value	IDI	p^c -value
Training	Imaging	0.944 (0.865–0.984)	0.405	93.75	88.14	89.33	78.95	0.775	0.004**	0.051	0.206
	Clinical	0.915 (0.828–0.967)	0.138	81.25	91.53	89.33	76.47	1.104	<0.001***	0.169	0.054
	Combined	0.961 (0.889–0.992)	/	87.50	93.22	92.00	82.35	/	/	/	/
Testing	Imaging	0.898 (0.732–0.978)	0.224	87.50	86.36	86.67	77.78	0.977	0.009**	0.065	0.250
	Clinical	0.869 (0.696–0.964)	0.356	87.50	77.27	80.00	70.00	1.227	<0.001***	0.157	0.092
	Combined	0.932 (0.777–0.991)	/	87.50	90.91	90.00	82.35	/	/	/	/
Validation	Imaging	0.886 (0.709–0.974)	0.241	83.33	81.82	82.14	66.67	0.545	0.221	0.072	0.145
	Clinical	0.841 (0.654–0.951)	0.225	100.00	68.18	75.00	63.16	0.970	0.021*	0.198	0.144
	Combined	0.917 (0.749–0.987)	/	83.33	90.91	89.29	76.92	/	/	/	/

p^a -value: AUC compared with combined model; p^b -value: continuous NRI compared with combined model; p^c -value: IDI compared with combined model. * $p < 0.05$ and ** $p < 0.01$. CI, confidence interval. AUC, area under the curve; CI, confidence interval; NRI, net reclassification index; IDI, integrated discrimination index.

**Figure 5.** Receiver operating characteristic curves and decision curve analysis of the imaging, clinical, and combined models for distinguishing between mild and moderate-to-severe renal interstitial fibrosis in the training (A, D), testing (B, E), and validation (C, F) sets.

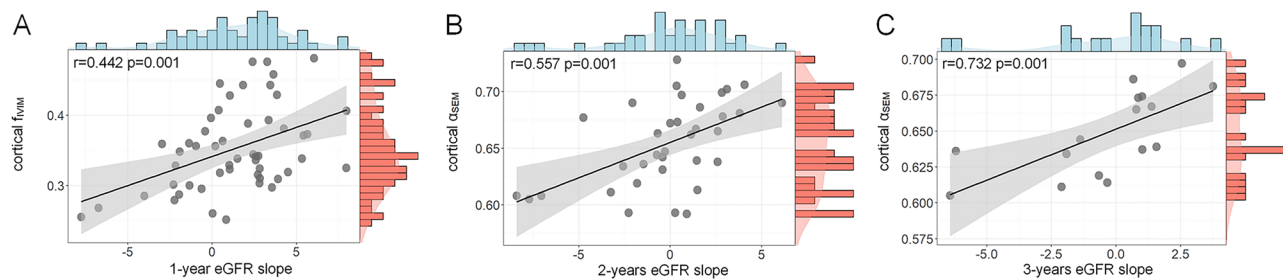


Figure 6. Correlations between diffusion model metrics and 1-, 2-, and 3-year eGFR slopes. eGFR, estimated glomerular filtration rate.

Table 6. Linear regression of diffusion metrics with eGFR slope.

Metric	Model 1			Model 2	
	β (95% CI)	p -value		β (95% CI)	p -value
1-year	Cortical f_{IVIM}	23.593 (10.009–37.177)	0.001**	30.600 (13.658–47.541)	0.001**
2-year	Cortical α_{SEM}	45.879 (20.251–71.508)	0.001**	44.859 (17.610–72.108)	0.002**
3-year	Cortical α_{SEM}	65.813 (25.528–106.099)	0.004**	95.631 (26.299–164.964)	0.019*

Model 1 is unadjusted. Model 2 is adjusted for age, sex, primary/secondary, angiotensin-converting enzyme inhibitor or angiotensin receptor blocker use, immunosuppressant use, baseline estimated glomerular filtration rate, 24-h urinary protein (ln-transformed), mean arterial pressure, and renal interstitial fibrosis score. β represents the unstandardized coefficients. * $p < 0.05$ and ** $p < 0.01$. CI, confidence interval.

In this study, an imaging model based on cortical f_{IVIM} and MK_{DKI} was constructed, highlighting the importance of reduced microcirculation perfusion and increased microstructural heterogeneity in IF grading. In clinical practice, eGFR and 24-h urinary protein are widely used laboratory indicators for assessing renal function and damage [27]. While both indicators were identified as independent factors for IF grading in our study, the clinical model they constituted did not outperform the imaging model in terms of AUC. In some cases, even with severe pathological damage to many nephrons, the filtration and compensatory hypertrophy of the remaining healthy nephrons can maintain normal eGFR levels [28,29], potentially compromising the clinical model's performance. Besides, the 24-h urinary protein collection process is complex and prone to errors in sample handling and analysis [30]. In contrast, the acquisition of f_{IVIM} and MK_{DKI} is stable [31,32] and showed good measurement consistency in our study. By integrating cortical f_{IVIM} , MK_{DKI} and eGFR, the combined model effectively reduces the bias and limitations associated with individual models, thereby enhancing overall diagnostic performance. This improvement is supported by the continuous NRI and DCA results, which show that the combined model achieved notable improvement across all datasets compared to the clinical model. The combined model serves as a comprehensive, noninvasive tool for accurately identifying IF severity, thereby aiding clinicians in developing individualized treatment and follow-up plans. Furthermore, the temporal external validation set demonstrated a similar performance to that of the testing set, suggesting the long-term stability of the model across different timepoints, ensuring robustness in future clinical applications.

We identified cortical f_{IVIM} and α_{SEM} as potential new non-invasive imaging biomarkers to predict short-term CKD progression. Our results revealed that lower cortical f_{IVIM} was associated with a faster 1-year eGFR decline. Chronic hypoxia, a key mechanism of CKD progression, may explain this result. f_{IVIM} is proportional to blood vessel density, which is linked to

the oxygen supply [33]. Loss of the microvascular system creates a hypoxic environment, leading to local inflammation and fibrosis. This, in turn, affects adjacent previously unaffected capillaries, nephrons, and glomeruli, exacerbating renal dysfunction, expanding the hypoxic area, and forming a vicious cycle [34]. Two prior reports found that reduced cortical oxygenation measured by blood oxygen level dependent-MRI was associated with progressive decline in kidney function in CKD patients [35,36], which also supports our findings. We also demonstrated an association between cortical α_{SEM} and the 2- and 3-year eGFR slopes. Although unrelated to renal IF, cortical α_{SEM} may be more sensitive to characterizing other factors associated with progression, such as inflammation [29]. The exact underlying biological mechanisms need further clarification. A previous study also explored the relationship between other DWI metrics and eGFR slope and found that ADC_{mono} and MK_{DKI} exhibited significant correlations with the eGFR slope [37]. However, we found no such association in our study. The method used to calculate the eGFR slope differed in that study. We used the linear mixed-effects model, whereas they used the two-point method or linear regression method. Additionally, different b-values used for model fitting may have affected the results. These discrepancies highlight the need for standardized methodologies.

Our study had several limitations. First, the sample size was relatively small, with a limited proportion of patients exhibiting severe fibrosis. Additionally, the models developed lacked multicenter external validation. Despite the numerous challenges faced by the coordination and reproducibility of multi-center diffusion MRI data [38], the reliability of the model can be verified in a prospective larger multi-center dataset by optimizing data coordination algorithms and establishing standardized processes in the future. Second, the accessibility of 3T-MRI machines is limited by cost and availability constraints in many healthcare settings. We plan to incorporate data from both 1.5T- and 3T-MRI in large-scale

studies, evaluating the model's performance across different equipment settings. This approach will enhance its clinical utility and benefit a more broader patient population. Third, integration of DWI with complementary MRI modalities enables a more comprehensive morphological and functional assessment of renal tissue. Future studies will also focus on exploring the added value of multimodal imaging approaches in evaluating CKD pathology and predicting disease progression.

Conclusion

A multi-b DWI scan, through different model calculations, can be used both to assess renal IF and 1–3-year eGFR decline. The combination of cortical f_{IVIM} , MK_{DKI} , and eGFR enables accurately and noninvasively identifying renal IF severity, aiding clinicians in optimizing treatment strategies and follow-up plans. Additionally, cortical f_{IVIM} and α_{SEM} show potential as imaging biomarkers for predicting short-term CKD progression, enabling personalized monitoring and prevention of adverse outcomes.

Disclosure statement

No potential conflict of interest was reported by the author(s).

Funding

This work was supported by the National Natural Science Foundation of China (grant number: 82371942).

References

- [1] Levin A, Ahmed SB, Carrero JJ, et al. Executive summary of the KDIGO 2024 clinical practice guideline for the evaluation and management of chronic kidney disease: known knowns and known unknowns. *Kidney Int.* 2024;105(4):684–701. doi: [10.1016/j.kint.2023.10.016](https://doi.org/10.1016/j.kint.2023.10.016).
- [2] Klinkhammer BM, Boor P. Kidney fibrosis: emerging diagnostic and therapeutic strategies. *Mol Aspects Med.* 2023;93:101206. doi: [10.1016/j.mam.2023.101206](https://doi.org/10.1016/j.mam.2023.101206).
- [3] Han M, Moon S, Lee S, et al. Novel genetic variants associated with chronic kidney disease progression. *J Am Soc Nephrol.* 2023;34(5):857–875. doi: [10.1681/ASN.0000000000000066](https://doi.org/10.1681/ASN.0000000000000066).
- [4] Wittsack HJ, Lanzman RS, Mathys C, et al. Statistical evaluation of diffusion-weighted imaging of the human kidney. *Magn Reson Med.* 2010;64(2):616–622. doi: [10.1002/mrm.22436](https://doi.org/10.1002/mrm.22436).
- [5] Mao C, Hu L, Jiang W, et al. Discrimination between human epidermal growth factor receptor 2 (HER2)-low-expressing and HER2-overexpressing breast cancers: a comparative study of four MRI diffusion models. *Eur Radiol.* 2024;34(4):2546–2559. doi: [10.1007/s00330-023-10198-x](https://doi.org/10.1007/s00330-023-10198-x).
- [6] Karaman MM, Zhang J, Xie KL, et al. Quartile histogram assessment of glioma malignancy using high b-value diffusion MRI with a continuous-time random-walk model. *NMR Biomed.* 2021;34(4):e4485. doi: [10.1002/nbm.4485](https://doi.org/10.1002/nbm.4485).
- [7] Rosenkrantz AB, Padhani AR, Chenevert TL, et al. Body diffusion kurtosis imaging: basic principles, applications, and considerations for clinical practice. *J Magn Reson Imaging.* 2015;42(5):1190–1202. doi: [10.1002/jmri.24985](https://doi.org/10.1002/jmri.24985).
- [8] Le Bihan D, Ichikawa S, Motosugi U. Diffusion and intra-voxel incoherent motion mr imaging-based virtual elastography: a hypothesis-generating study in the liver. *Radiology.* 2017;285(2):609–619. doi: [10.1148/radiol.2017170025](https://doi.org/10.1148/radiol.2017170025).
- [9] Sun K, Zhu Y, Chai W, et al. Diffusion-weighted MRI-based virtual elastography and shear-wave elastography for the assessment of breast lesions. *J Magn Reson Imaging.* 2024;60(5):2207–2213. doi: [10.1002/jmri.29302](https://doi.org/10.1002/jmri.29302).
- [10] Hua C, Qiu L, Zhou L, et al. Value of multiparametric magnetic resonance imaging for evaluating chronic kidney disease and renal fibrosis. *Eur Radiol.* 2023;33(8):5211–5221. doi: [10.1007/s00330-023-09674-1](https://doi.org/10.1007/s00330-023-09674-1).
- [11] Kromrey ML, Le Bihan D, Ichikawa S, et al. Diffusion-weighted MRI-based virtual elastography for the assessment of liver fibrosis. *Radiology.* 2020;295(1):127–135. doi: [10.1148/radiol.2020191498](https://doi.org/10.1148/radiol.2020191498).
- [12] Inker LA, Collier W, Greene T, et al. A meta-analysis of GFR slope as a surrogate endpoint for kidney failure. *Nat Med.* 2023;29(7):1867–1876. doi: [10.1038/s41591-023-02418-0](https://doi.org/10.1038/s41591-023-02418-0).
- [13] Levey AS, Stevens LA, Schmid CH, et al. A new equation to estimate glomerular filtration rate. *Ann Intern Med.* 2009;150(9):604–612. doi: [10.7326/0003-4819-150-9-200905050-00006](https://doi.org/10.7326/0003-4819-150-9-200905050-00006).
- [14] Sugawara Y, Kanda E, Ohsugi M, et al. eGFR slope as a surrogate endpoint for end-stage kidney disease in patients with diabetes and eGFR > 30 mL/min/1.73 m² in the J-DREAMS cohort. *Clin Exp Nephrol.* 2024;28(2):144–152. doi: [10.1007/s10157-023-02408-z](https://doi.org/10.1007/s10157-023-02408-z).
- [15] Grams ME, Sang Y, Ballew SH, et al. Evaluating glomerular filtration rate slope as a surrogate end point for ESKD in clinical trials: an individual participant meta-analysis of observational data. *J Am Soc Nephrol.* 2019;30(9):1746–1755. doi: [10.1681/ASN.2019010008](https://doi.org/10.1681/ASN.2019010008).
- [16] Leung G, Kirpalani A, Szeto SG, et al. Could MRI be used to image kidney fibrosis? A review of recent advances and remaining barriers. *Clin J Am Soc Nephrol.* 2017;12(6):1019–1028. doi: [10.2215/CJN.07900716](https://doi.org/10.2215/CJN.07900716).
- [17] Hu W, Dai Y, Liu F, et al. Assessing renal interstitial fibrosis using compartmental, non-compartmental, and model-free diffusion MRI approaches. *Insights Imaging.* 2024;15(1):156. doi: [10.1186/s13244-024-01736-2](https://doi.org/10.1186/s13244-024-01736-2).
- [18] Yan Z, Chen L, Shen W, et al. Preliminary study on intra-voxel incoherent motion imaging and diffusion kurtosis imaging based on magnetic resonance imaging of normal kidneys in children. *Transl Pediatr.* 2022;11(12):1928–1938. doi: [10.21037/tp-22-558](https://doi.org/10.21037/tp-22-558).
- [19] Le Bihan D. What can we see with IVIM MRI? *Neuroimage.* 2019;187:56–67. doi: [10.1016/j.neuroimage.2017.12.062](https://doi.org/10.1016/j.neuroimage.2017.12.062).
- [20] Anderson SW, Barry B, Soto J, et al. Characterizing non-gaussian, high b-value diffusion in liver fibrosis: stretched exponential and diffusional kurtosis modeling.

- J Magn Reson Imaging. 2014;39(4):827–834. doi: [10.1002/jmri.24234](https://doi.org/10.1002/jmri.24234).
- [21] Zhong G, Chen L, Lin Z, et al. Evaluation of renal function in chronic kidney disease using histogram analysis based on multiple diffusion models. *Br J Radiol*. 2024;97(1156):803–811. doi: [10.1093/bjr/tqae024](https://doi.org/10.1093/bjr/tqae024).
- [22] Zhang S, Lin Y, Ge X, et al. Multiparameter diffusion-weighted imaging for characterizing pathological patterns in lupus nephritis patients: a preliminary study. *J Magn Reson Imaging*. 2019;50(4):1075–1084. doi: [10.1002/jmri.26657](https://doi.org/10.1002/jmri.26657).
- [23] Zhou XJ, Gao Q, Abdullah O, et al. Studies of anomalous diffusion in the human brain using fractional order calculus. *Magn Reson Med*. 2010;63(3):562–569. doi: [10.1002/mrm.22285](https://doi.org/10.1002/mrm.22285).
- [24] Sui Y, Xiong Y, Jiang J, et al. Differentiation of low- and high-grade gliomas using high b-value diffusion imaging with a non-Gaussian diffusion model. *AJNR Am J Neuroradiol*. 2016;37(9):1643–1649. doi: [10.3174/ajnr.A4836](https://doi.org/10.3174/ajnr.A4836).
- [25] Du M, Zou D, Gao P, et al. Evaluation of a continuous-time random-walk diffusion model for the differentiation of malignant and benign breast lesions and its association with Ki-67 expression. *NMR Biomed*. 2023;36(8):e4920. doi: [10.1002/nbm.4920](https://doi.org/10.1002/nbm.4920).
- [26] Novikov DS, Kiselev VG, Jespersen SN. On modeling. *Magn Reson Med*. 2018;79(6):3172–3193. doi: [10.1002/mrm.27101](https://doi.org/10.1002/mrm.27101).
- [27] Stevens PE, Ahmed SB, Carrero JJ, et al. KDIGO 2024 clinical practice guideline for the evaluation and management of chronic kidney disease. *Kidney Int*. 2024;105(4):S117–S314. doi: [10.1016/j.kint.2023.10.018](https://doi.org/10.1016/j.kint.2023.10.018).
- [28] Ge XY, Lan ZK, Lan QQ, et al. Diagnostic accuracy of ultrasound-based multimodal radiomics modeling for fibrosis detection in chronic kidney disease. *Eur Radiol*. 2023;33(4):2386–2398. doi: [10.1007/s00330-022-09268-3](https://doi.org/10.1007/s00330-022-09268-3).
- [29] Ruiz-Ortega M, Rayego-Mateos S, Lamas S, et al. Targeting the progression of chronic kidney disease. *Nat Rev Nephrol*. 2020;16(5):269–288. doi: [10.1038/s41581-019-0248-y](https://doi.org/10.1038/s41581-019-0248-y).
- [30] Zhao YF, Zhu L, Liu LJ, et al. Measures of urinary protein and albumin in the prediction of progression of IgA nephropathy. *Clin J Am Soc Nephrol*. 2016;11(6):947–955. doi: [10.2215/CJN.10150915](https://doi.org/10.2215/CJN.10150915).
- [31] Kemėšienė J, Rühle A, Gomolka R, et al. Advanced diffusion imaging of abdominal organs in different hydration states of the human body: stability of biomarkers. *Heliyon*. 2021;7(1):e06072. doi: [10.1016/j.heliyon.2021.e06072](https://doi.org/10.1016/j.heliyon.2021.e06072).
- [32] Chen J, Zhang Z, Liu J, et al. Multiparametric magnetic resonance imaging of the kidneys: effects of regional, side, and hydration variations on functional quantifications. *J Magn Reson Imaging*. 2023;57(5):1576–1586. doi: [10.1002/jmri.28477](https://doi.org/10.1002/jmri.28477).
- [33] Chen Z, Xue Y, Zhang Z, et al. The performance of intravoxel-incoherent motion diffusion-weighted imaging derived hypoxia for the risk stratification of prostate cancer in peripheral zone. *Eur J Radiol*. 2020;125:108865. doi: [10.1016/j.ejrad.2020.108865](https://doi.org/10.1016/j.ejrad.2020.108865).
- [34] Fine LG, Norman JT. Chronic hypoxia as a mechanism of progression of chronic kidney diseases: from hypothesis to novel therapeutics. *Kidney Int*. 2008;74(7):867–872. doi: [10.1038/ki.2008.350](https://doi.org/10.1038/ki.2008.350).
- [35] Zhou H, Yang M, Jiang Z, et al. Renal hypoxia: an important prognostic marker in patients with chronic kidney disease. *Am J Nephrol*. 2018;48(1):46–55. doi: [10.1159/000491551](https://doi.org/10.1159/000491551).
- [36] Pruijm M, Milani B, Pivin E, et al. Reduced cortical oxygenation predicts a progressive decline of renal function in patients with chronic kidney disease. *Kidney Int*. 2018;93(4):932–940. doi: [10.1016/j.kint.2017.10.020](https://doi.org/10.1016/j.kint.2017.10.020).
- [37] Liu Y, Zhang GM, Peng X, et al. Diffusion kurtosis imaging as an imaging biomarker for predicting prognosis in chronic kidney disease patients. *Nephrol Dial Transplant*. 2022;37(8):1451–1460. doi: [10.1093/ndt/gfab229](https://doi.org/10.1093/ndt/gfab229).
- [38] Afzali M, Pieciak T, Newman S, et al. The sensitivity of diffusion MRI to microstructural properties and experimental factors. *J Neurosci Methods*. 2021;347:108951. doi: [10.1016/j.jneumeth.2020.108951](https://doi.org/10.1016/j.jneumeth.2020.108951).